Proceedings of the 21st ICSMGE, Vienna, Austria, 14 – 19 June 2026. Pistrol, Adam & Schweiger (eds.)
Published by: ÖGG, Austrian Society for Geomechanics, Salzburg, Austria, ISBN 978-3-9503898-4-5
https://doi.org/10.53243/ICSMGE2026-1065

Clay content influence on static behavior of silty sands at low confining stress

Davor Marušić, Vedran Jagodnik
University of Rijeka, Faculty of Civil Engineering, Croatia, davor.marusic@uniri.hr

ABSTRACT: Silty sands represent the two-component soil mixtures with a dominant proportion of incoherent sand and an inferior proportion of coherent silt, sometimes clay. The dominant proportion of sand is most often defined by the granular structure of the soil, where sand grains are in contact with each other, which determines the behavior of the soil in static and dynamic conditions. Such conditions should dominate until the so-called "fines threshold", where the fine-grained component assumes the role of the load-bearing structure of the soil while the sand grains "float" in the fine-grained matrix (sandy silts). The static behavior of silty sands is commonly researched using the static triaxial shear test, which subjects the isotropically confined specimens to diverse stress-path loading. Sampling the relatively cohesionless sandy soils for the triaxial shear tests proved difficult, and silty sand specimens are usually reconstituted using representative natural soil sediments or artificial mixtures. Research has shown that certain physical characteristics of silty sands differ significantly from those of the host sand and change with the change in the fines content. The void ratios are used with phase relations to determine the mass fractions of solids and water used to reconstitute the sand specimen within a certain volume at a predetermined relative density. However, the void ratios of silty sands significantly vary with the mineral composition and the size of the fine-grained component. Existing analytical models have been successfully used to redefine relative density and silty sands' minimum and maximum void ratios. The present research examines the change in the behavior of silty sands at low effective stresses with a change in the fines content. Using the redefined physical characteristics of silty sands, the relative density of individual mixtures has been determined more precisely, enabling better control and evaluation of static test results.

KEYWORDS: Silty sand, kaolinite clay, relative density, triaxial compression, low effective stress.

1 INTRODUCTION

This study investigates the behaviour of clayey and silty sand under low confining pressures, under static drained and undrained conditions. The tested silty sand mixtures (Figure 1) were reconstituted using "Modland" uniform quartz sand, combined with kaolinite clay and silt as the fines component, and then subjected to monotonic triaxial compression testing.

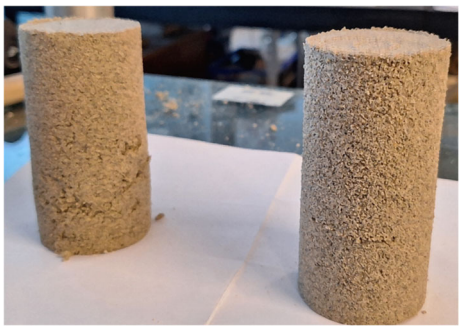

Figure 1. Physical appearance of the reconstituted silty sand mixture.

1.1 *Sand void ratio and relative density*

For reconstituted granular soils, a key control parameter is the relative density (D_r), defined in Equation (1) as a relative position between the minimum and maximum void ratios (the densest and loosest possible soil states, respectively).

$$D_r = \frac{e_{max} - e}{e_{max} - e_{min}} \cdot 100\% \quad (1)$$

where:

- D_r – relative density
- e – specimen's void ratio (global void ratio)
- e_{min} – specimen's minimum void ratio
- e_{max} – specimen's maximum void ratio

The void ratios given by phase relations represent important physical soil parameters that define the volumetric change and relative density of the granular soil.

1.2 *Sand-fines mixtures' void ratio and relative density*

Determining physical properties in mixtures of sand and fines, especially those including plastic clays, is challenging due to the distinct behaviours of each fraction. Existing standards (ASTM D4253-14, 2014; ASTM D4254-14, 2014); are primarily applicable to non-plastic, free-draining silty sands. However, the kaolinite clay used in this study introduces plasticity and impairs drainage, demanding an alternative approach to define void ratios.

1.3 *Intergranular void ratio of binary mixtures*

Studies by (Lade et al., 1998; Thevanayagam, 1998) indicate that fines in silty sands may either occupy voids within the sand matrix and lower the overall void ratio, or bridge between sand grains, altering structural force chains and increase void ratios (Thevanayagam et al., 2002). These effects are schematically presented in Figure 2.

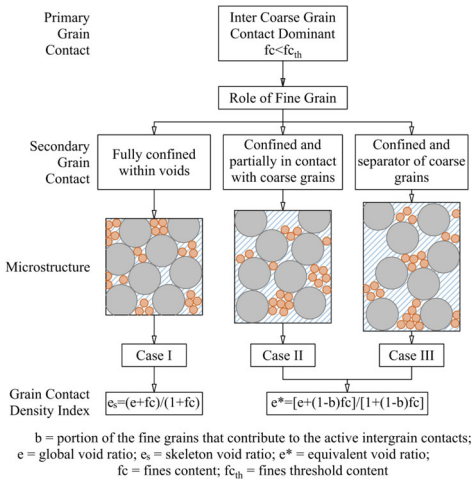

Figure 2. Intergranular soil mix classification for coarse-grain soil mix - adopted and modified from (Thevanayagam et al., 2002).

1.4 *Analythical void ratio determination method*

(Chang, Wang and Ge, 2015; 2016) proposed an analytical method to redefine minimum and maximum void ratios in silty sands, which has since been validated in later research (Chang, Wang and Ge, 2016; Polito, 2023). The minimum void ratio for a sand-fines mixture (e_m^{min}) is calculated using Equation (2):

$$e_m^{min} = e_s^{min} \cdot y_s + e_f^{min} \cdot y_f - a \cdot (1 + e_f^{min}) \cdot y_f \qquad (2)$$

where:

- e_m^{min}, – minimum void ratio of the mixture
- e_s^{min}, e_f^{min} – sand, fines fraction minimum void ratio
- y_s, y_f – sand, fines fraction volume content
- a – filling coefficient

Considering the linear relationship between the e_{min} and e_{max}, an Equation (3), a corresponding equation for silty sand'maximum void ratio (e_m^{max}) is also provided by (Chang, Wang and Ge, 2016).

$$e_m^{max} = \alpha \cdot e_m^{min} + \beta \qquad (3)$$

where:

- e_m^{min} – minimum void ratio of the mixture
- e_m^{max} – maximum void ratio of the mixture
- α, β – constant parameters

With α and β calculated in Equations (4) and (5):

$$\alpha = \frac{e_s^{max} - e_f^{max} + a \cdot (1 + e_f^{max})}{e_s^{min} - e_f^{min} + a \cdot (1 + e_f^{min})} \qquad (4)$$

$$\beta = e_s^{max} - \alpha \cdot e_s^{min} \qquad (5)$$

This method was adopted to estimate void ratios in the silty sand mixtures examined in this research.

2 METHODOLOGY

2.1 *Silty sands' physical properties*

The silty sand samples were produced by combining quartz sand and kaolinite in set mass ratios. Table 1 summarises their physical properties, previously documented (Marušić and Jagodnik, 2023; 2025; Jagodnik et al., 2024).

Table 1. Soil specimens' physical properties.

Soil type		SK0	SK10	SK15	SK100
Mass percentage of sand/kaolinite fraction		100/0	90/10	85/15	0/100
Specific gravity	G_s $[g/cm^3]$	2.70	2.69	2.67	2.60
Effective particle size	D_{50} [mm]	0.289	0.276	0.270	0.005
Liquid limit	LL [%]	N/A	N/A	N/A	53
Plastic limit	PL [%]	N/A	N/A	N/A	30

2.2 *Alternative void ratios determination*

Using Equation (2), the alternative void ratios for SK10 and SK15 mixtures were analytically determined (Chang, Wang and Ge, 2015; 2016). Since direct experimental validation was not feasible, the filling coefficient (a) was estimated using a fitted power function – Equation (6), derived from the existing test data (Chang, Wang and Ge, 2015).

$$a = (1 - d_{50}/D_{50})^p \qquad (6)$$

The best-fit curve with the corresponding p-value was obtained using the complete available data set.

The fitted power trend and obtained parameters were then used to calculate the minimum, and subsequently the maximum void ratio with Equations (3), (4), and (5).

Specimens reconstituted this way were further evaluated with the triaxial test results and correlated with the existing test results.

2.3 *Specimen preparation*

Samples were prepared in latex membranes using a 50 mm × 100 mm cylindrical mold. The undercompaction method (Ladd, 1978) with 5% undercompaction was used, targeting a relative density of 80%, guided by the alternative void ratio (Chang, Wang and Ge, 2015; 2016) calculations.

2.4 *Monotonic compression*

Triaxial compression tests were conducted at the University of Rijeka, Faculty of Civil Engineering's Geotechnical Lab, following (ASTM D7181-20, 2020) and (ASTM D4767-11, 2020) standards.

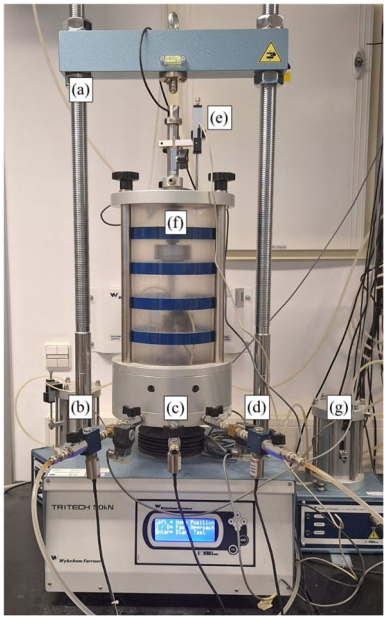

Figure 3. Triaxial system used.

The triaxial system, shown in Figure 3, operated through a computer-controlled system. The triaxial system consists of triaxial frame (Figure 3(a)) and uses transducers to measure the cell (Figure 3(b)), pore (Figure 3(c)), and back pressures (Figure 3(d)) during the saturation, consolidation, and shear phases. The vertical linear variable differential (Figure 3(e)) transducer (LVDT) measures the vertical displacement during the test while the vertical force is measured with the submerged load cell (Figure 3(f)). Volumetric change is tracked with the volume change device (Figure 3(g)). The membrane corrections were introduced into the analysis (Lade, 2016; ASTM D7181-20, 2020). The computer-controlled system records the test data and automatically manipulates the targeted pressures and loads during the test.

Drained and undrained, strain-controlled triaxial compression tests were performed at low effective confining pressures (25 and 50 kPa), using a 4% axial strain rate.

Saturation involved three stages: CO_2 percolation, de-aired water percolation, and increasing back pressure increments, achieving a B-value of 0.95 to ensure full saturation.

For all tests performed, the isotropic consolidation was performed in a single stage due to low resulting hydraulic gradients at targeted low confining stresses.

3 RESULTS

3.1 *Void ratio determination*

The existing analytical approach (Chang, Wang and Ge, 2015; 2016) was used to redefine the mixtures' minimum and maximum void ratios. The minimum void ratio is obtained with Eguation (2), by determining the mixture's specific parameters a and p, defined in Equation (6).

Since the mixtures' void ratio values could not be physically determined, the complete available data set (Chang, Wang and Ge, 2015) was used to obtain the best-fit curve with the corresponding p parameter and a coefficient, shown in Figure 4.

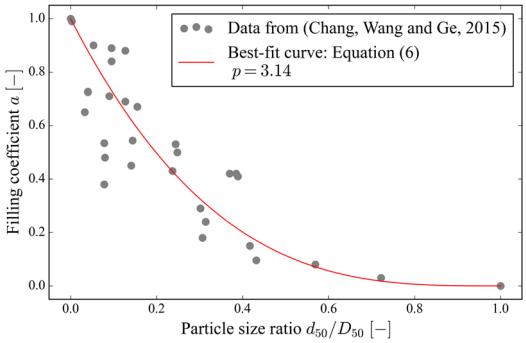

Figure 4. The filling coefficient (a) relation to a particle size ratio (d_{50}/D_{50}), and the computed best-fit power trend.

With the obtained p parameter, the a coefficient, and the corresponding minimum void ratio, the maximum void ratio was obtained with Equation (3), using the parameters α and β defined in Equations (4) and (5). The obtained parameters are listed in (Chang, Wang and Ge, 2016) Table 2 and the determined void ratios are presented in Table 3.

Table 2. Determined silty sand mixtures' parameters, used for void ratios determination.

d_{50}/D_{50}	p	a	α	β
0.014	3.14	0.957	1.151	0.173

Table 3. Soil specimens' void ratios.

Soil type		SK0	SK10	SK15	SK100
Minimum void ratio	e_{min} [−]	0.641	0.479	0.399	0.780
Maximum void ratio	e_{max} [−]	0.911	0.725	0.632	1.378

The value of the filling coefficient $a = 0.957 \approx 1$, approximates the limiting case condition with all the fines filling the host sand pore spaces, and none participating in the mixture's structure. This condition can also be identified as the intergranular (Thevanayagam, 1998) or the skeleton (Yang, Wei and Dai, 2015) void ratio. It relates well to case I condition shown in Figure 2, with the mean particle sizes of sand and fines $D_{50}/d_{50} > 6.5$ for spherical particles (Thevanayagam et al., 2002), and to the filling coefficient's power trend relation to a particle size ratio shown in Figure 4.

3.2 *Drained monotonic compression tests*

A total of 10 drained monotonic compression tests were performed on SK10 and SK15 mixtures and the host sand (SK0) specimens. The quantitative results of the drained compression tests are summarised in Table 4.

Table 4. Consolidated drained triaxial test results.

Soil type	Initial conditions		Peak state	Critical state		
	e_0 [−]	$p'0$ $[kPa]$	q/p' $[kPa]$	e_c [−]	p' $[kPa]$	q/p' $[kPa]$
SK0	0.695	25	1.454	0.693	42.55	1.096
SK0	0.695	50	1.545	0.690	88.17	1.265
SK10	0.522	25	1.663	0.519	44.59	1.313
SK10	0.522	50	1.536	0.519	80.89	1.270
SK15	0.436	25	1.677	0.435	56.00	1.250
SK15	0.436	50	1.683	0.434	100.00	1.333

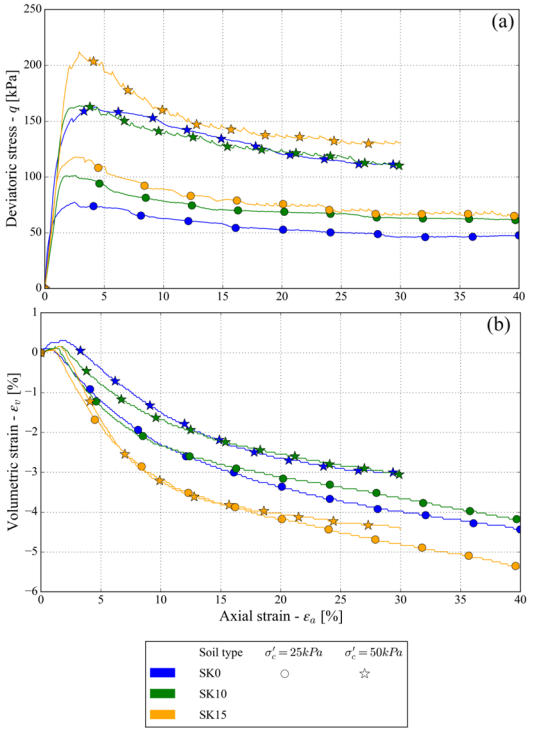

Figure 5. Deviatoric stress – q (**a**) and volumetric strain – ε_v (**b**) relation to axial strain – ε_a in the drained triaxial compression

For all specimens tested, the peak deviatoric stress was reached within 2-4% of axial strain, shown in Figure 5(a). At higher axial strains, the deviatoric stress begins to drop to a critical state value at approximately 30% axial strain. The SK15 specimens exhibited a slightly higher deviatoric stress increase than the host sand and SK10 specimens at 25 and 50 kPa initial confining stresses. The SK10 also exhibited a slightly higher deviatoric stress increase than the host sand at 25 kPa initial confining stress, while at the 50 kPa initial confining stress, the SK10 and host sand showed similar deviatoric stress to axial strain relation. Specimens initially undergo compression in the early stages of axial loading, shown in Figure 5(b). The highest positive volumetric strain of 0.3% at 2% axial strain is recorded for the host sand tested at 50 kPa confining stress. Silty sand mixtures initially exhibited smaller volumetric strain than the host sand at 50 kPa confining stress. After initial compression, the volumetric strain begins to drop with an increased negative value at higher axial strains as the specimens undergo constant dilation. The SK15 specimens at 25 and 50 kPa initial confining stresses resulted in the highest negative volumetric strain. The host sand and SK10 specimens show similar dilative behaviour, which increases at lower confining stress.

The host sand and mixtures exhibited initial compression at very low axial strains and dilation with decreasing negative volumetric strain at higher axial strains, a characteristic of medium-dense and dense sand specimens.

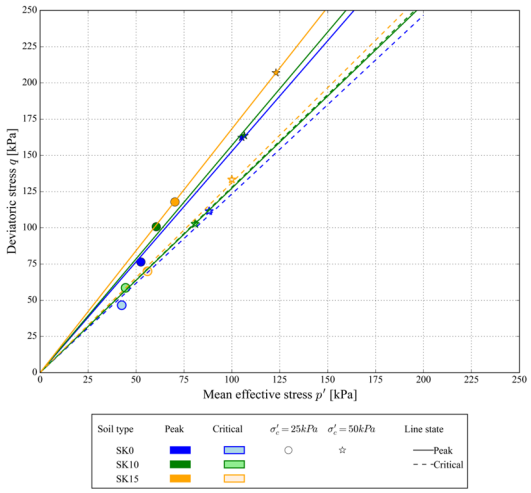

Figure 6. Drained stress-path presentation of peak and critical state values with assumed corresponding lines

The SK15 specimen reaches consistently higher peak and critical values of q and p' than the host sand, and the SK10 reaches relatively similar values to those of the host sand at 50kPa confining stress, and higher values at 25kPa confining stress, as presented in Figure 6.

Since the specimens tested were fully saturated, the water content surpassed the clay fraction's liquid limit. With consequential loss of cohesive forces, the unfavourable slip and flow mechanisms will govern the specimen's clay fraction in drained conditions, with the potential of selective particle migration (internal erosion or suffusion) and loss of specimen homogeneity. Regarding the mixtures, a small change in soil behaviour with a change in fines content could be attributed to the specimen's varying relative density due to the inaccurately analytically determined void ratios, to the changing clay consistency at different saturation degrees, or the potential structural rearrangement of the clay fraction during the test (loss of specimen homogeneity).

3.3 *Undrained monotonic compression tests*

A total of 10 undrained monotonic compression tests were performed on SK10 and SK15 mixtures and the host sand (SK0) specimens. The quantitative results of the undrained compression tests are summarised in Table 5.

Table 5. Consolidated undrained triaxial test results

Specimen type	Initial conditions		Steady state	
	e_0 [−]	$p'0$ $[kPa]$	p' $[kPa]$	q $[kPa]$
SK0	0.695	25	425.68	605.05
SK0	0.695	50	435.49	630.03
SK10	0.522	25	383.14	486.42
SK10	0.522	50	574.56	769.69
SK15	0.436	25	647.11	891.32
SK15	0.436	50	729.41	1033.24

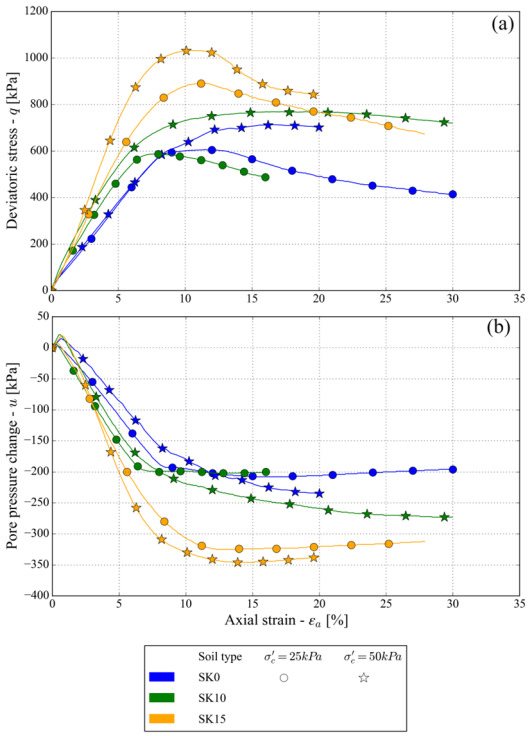

Figure 7. Deviatoric stress – q (**a**) and pore water pressure change – u (**b**) relation to axial strain – ε_a in the undrained triaxial compression.

For all specimens tested, the peak deviatoric stress was reached within 7-15% of axial strain, shown in Figure 7(a). With increasing axial strains, the deviatoric stress gradually declines. In the early stages of axial loading (up to 1% axial strain), specimens initially show a positive pore pressure change, presented in Figure 7(b) . The initial pore water pressure increase is unaffected by the fines content. With increasing axial strain, the pore water pressure changes drop to a constant negative value at approximately 7-25% axial strain. The decrease in the rate and value of pore water pressure is affected by the fines content but is unaffected by changing confining stresses. The higher the fines content, the higher the increase in negative pore pressure.

The initial pore water pressure increase, followed by a decrease to a constant negative value with increasing axial strain, indicates an initial compression followed by dilation, a characteristic of dense and mid-dense sands.

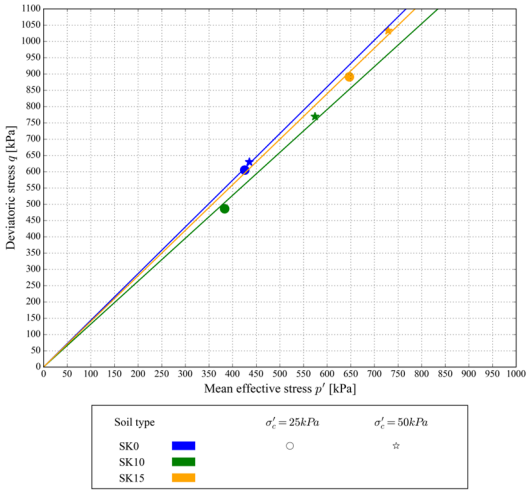

Figure 8. Undrained stress-path presentation of the determined steady state lines for each specimen type

For specimens tested at 50 kPa initial confining stress, the steady state q and p' values increase with an increase in fines content, shown in Figure 8. At the 25 kPa initial confining stress, the SK15 specimen reaches higher values of q and p' than the host sand, and the SK10 reaches lower values to those of the host sand.

A small change in soil behaviour with a change in fines content could be attributed to the specimen's varying relative density due to the inaccurately determined void ratios, or the changing clay consistency at different saturation degrees.

4 CONCLUSIONS

Present research used the redefined the minimum and maximum void ratios of SK10 and SK15 sand-clay mixtures using the analytical approach of Chang, Wang, and Ge (2015, 2016), due to the inability to measure them directly. The resulting filling coefficient ($a \approx 1$) reflects a limiting case where fines occupy sand pore spaces without structural force transfer contribution, which is consistent with intergranular void ratio theory.

In drained monotonic compression tests, all specimens (SK0, SK10, SK15) showed early compression followed by dilation, typical of medium-dense to dense sands. SK15 consistently achieved higher peak and critical deviatoric stresses than host sand, particularly at lower confining stresses. SK10 performed similarly to or slightly above host sand depending on confining pressure. Mixture behaviour differences were small and may stem from inaccuracies in analytically determined void ratios, fines' clay consistency changes under saturation, or internal structural rearrangements during testing.

In undrained monotonic compression tests, specimens exhibited initial positive pore pressure (compression) followed by a drop to constant negative values (dilation), also characteristic of dense sands. Higher fines content increased the magnitude of negative pore pressures. At 50 kPa confining stress, steady-state strength increased with fines content, while at 25 kPa, SK15 exceeded and SK10 fell below host sand strength. Behavioural variations with fines content were again likely linked to relative density estimation errors and clay consistency changes.

SK15 mixtures generally outperformed host sand in both drained and undrained tests, especially at lower confining stresses, while SK10 showed mixed results. Variations in behaviour were likely influenced by combination of void ratio estimation errors and the intensity of clay consistency changes under saturation.

5 ACKNOWLEDGEMENTS

The tests were conducted in the Geotechnical Laboratory at the Faculty of Civil Engineering, University of Rijeka, within the Project Research Infrastructure for Campus-based Laboratories at the University of Rijeka, (RC.2.2.06-0001) funded by Ministry of Science, Education and Sports of the Republic of Croatia. This project has been co-funded by the European Fund for Regional Development (ERDF); this support is gratefully acknowledged.

The research was funded by the University of Rijeka, Croatia through the project "Physical and laboratory tests of interparticle behavior of sand and clay mixtures at low overburden stresses" (uniri-iskusni-tehnic-23- 183 212).

6 REFERENCES

Andrade, F.A., Al-Qureshi, H.A. and Hotza, D., 2011. Measuring the plasticity of clays: A review. Applied Clay Science, 51(1–2), pp.1–7. https://doi.org/10.1016/j.clay.2010.10.028.

Arbanas, Ž., Peranić, J., Jagodnik, V., Vivoda Prodan, M. and Čeh, N., 2023. Remedial Measures Impact on Slope Stability and Landslide Occurrence in Small-Scale Slope Physical Model in 1 g Conditions. In: I. Alcántara-Ayala, Ž. Arbanas, D. Huntley, K. Konagai, S. Mihalić Arbanas, M. Mikoš, M. V. Ramesh, K. Sassa, S. Sassa, H. Tang and B. Tiwari, eds. Progress in Landslide Research and Technology, Volume 2 Issue 2, 2023, Progress in Landslide Research and Technology. [online] Cham: Springer Nature Switzerland. pp.197–220. https://doi.org/10.1007/978-3-031-44296-4_9.

ASTM D4253-14, 2014. Standard Test Methods for Maximum Index Density and Unit Weight of Soils Using a Vibratory Table.

ASTM D4254-14, 2014. Standard Test Methods for Minimum Index Density and Unit Weight of Soils and Calculation of Relative Density.

ASTM D4767-11, 2020. Standard Test Method for Consolidated Undrained Triaxial Compression Test for Cohesive Soils.

ASTM D7181-20, 2020. Standard Test Method for Consolidated Drained Triaxial Compression Test for Soils.

Chang, C.S., Wang, J.-Y. and Ge, L., 2015. Modeling of minimum void ratio for sand–silt mixtures. Engineering Geology, 196, pp.293–304. https://doi.org/10.1016/j.enggeo.2015.07.015.

Chang, C.S., Wang, J.Y. and Ge, L., 2016. Maximum and minimum void ratios for sand-silt mixtures. Engineering Geology, 211, pp.7–18. https://doi.org/10.1016/j.enggeo.2016.06.022.

Jagodnik, V., Marušić, D., Arbanas, Ž., Čeh, N., Peranić, J. and Vivoda Prodan, M., 2024. Fines Content Influence on the Dynamic Slope Behavior in Small-Scale Physical Models. [online] pp.219–224. https://doi.org/10.18485/resylab.2024.6.ch32.

Ladd, R.S., 1978. Preparing Test Specimens Using Undercompaction. GEOTECHNICAL TESTING JOURNAL.

Lade, P., Chaney, R., Demars, K., Liggio, C. and Yamamuro, J., 1998. Effects of Non-Plastic Fines on Minimum and Maximum Void Ratios of Sand. Geotechnical Testing Journal, 21(4), p.336. https://doi.org/10.1520/GTJ11373J.

Lade, P.V., 2016. Triaxial testing of soils. Chichester, West Sussex: Wiley Blackwell.

Marušić, D. and Jagodnik, V., 2023. Determination of the Atterberg limits using a Fall Cone device on low plasticity silty sands. Rudarsko-geološko-naftni zbornik, 38(3), pp.133–145. https://doi.org/10.17794/rgn.2023.3.11.

Marušić, D. and Jagodnik, V., 2025. Atterberg limits determination and soil classification using Fall cone device on the silty sands and sandy silts. International Journal of Geotechnical Engineering, 19(1–3), pp.78–87. https://doi.org/10.1080/19386362.2025.2454655.

Mijic, Z., Bray, J.D., Riemer, M.F., Cubrinovski, M. and Rees, S.D., 2021. Test method for minimum and maximum densities of small quantities of soil. Soils and Foundations, 61(2), pp.533–540. https://doi.org/10.1016/j.sandf.2020.12.003.

Polito, C.P., 2023. Models for Estimating Coefficients for the Prediction of Maximum and Minimum Index Void Ratios for Mixtures of Sand and Non-Plastic Silt. [preprint] Engineering. https://doi.org/10.20944/preprints202309.1306.v1.

Prodan, M.V., Peranić, J., Pajalić, S., Jagodnik, V., Čeh, N. and Arbanas, Ž., 2022. Mechanism of rainfall induced landslides in small-scale models built of different materials.

Thevanayagam, S., 1998. Effect of Fines and Confining Stress on Undrained Shear Strength of Silty Sands. Journal of Geotechnical and Geoenvironmental Engineering, 124(6), pp.479–491.

Thevanayagam, S., Shenthan, T., Mohan, S. and Liang, J., 2002. Undrained Fragility of Clean Sands, Silty Sands, and Sandy Silts. Journal of Geotechnical and Geoenvironmental Engineering, 128(10), pp.849–859. https://doi.org/10.1061/(ASCE)1090-0241(2002)128:10(849).

Yang, J., Wei, L.M. and Dai, B.B., 2015. State variables for silty sands: Global void ratio or skeleton void ratio? *Soils and Foundations*, 55(1), pp.99–111. https://doi.org/10.1016/j.sandf.2014.12.008.